

Underwater Image Color Correction using Exposure-Bracketing Imaging

Kohei Nomura, Daisuke Sugimura, *Member, IEEE*, and Takayuki Hamamoto, *Member, IEEE*,

Abstract—Absorption and scattering of light in an underwater scene saliently attenuate red spectrum components. They cause heavy color distortions in the captured underwater images. In this letter, we propose a method for color-correcting underwater images, utilizing a framework of gray information estimation for color constancy. The key novelty of our method is to utilize exposure-bracketing imaging: a technique to capture multiple images with different exposure times for color correction. The long-exposure image is useful for sufficiently acquiring red spectrum information of underwater scenes. In contrast, pixel values in the green and blue channels in the short-exposure image are suitable because they are unlikely to attenuate more than the red ones. By selecting appropriate images (i.e., least over- and under-exposed images) for each color channel from those taken with exposure-bracketing imaging, we fuse an image that includes sufficient spectral information of underwater scenes. The fused image allows us to extract reliable gray information of scenes; thus, effective color corrections can be achieved. We perform color correction by linear regression of gray information estimated from the fused image. Experiments using real underwater images demonstrate the effectiveness of our method.

Index Terms—Underwater image, Color correction, Exposure bracketing imaging.

I. INTRODUCTION

THE development of underwater imaging techniques has attracted considerable attentions in recent years. However, absorption and scattering of light in an underwater scene cause heavy color distortion, making it difficult to recognize and analyze objects. If underwater images can be corrected to one of a canonical (i.e., white) illumination environment, they can contribute to marine biology progress. Thus, the aim of this study is correcting color distortions of underwater images.

The mechanisms of color distortions of underwater images are described as follows. Because of absorption and scattering, light spectrum components corresponding to wavelengths ranging from 600 to 700 nm (i.e., red light) particularly attenuate compared to those of other wavelengths [1]. In addition, the amount of color distortion in underwater images increases as the traveling distance of light to the camera increases. Thus, the amount of color distortion varies spatially depending on the scene depth in the image.

To address underwater imaging problems, many researchers have attempted restoring images by extending the optical imaging models of the air to underwater scenes [2]. With their imaging models, they restored underwater images using

K. Nomura and T. Hamamoto are with the Graduate School of Engineering, Tokyo University of Science, Tokyo, Japan (E-mail: {kouhei@isl.ee.kagu.tus.ac.jp; hamamoto@ee.kagu.tus.ac.jp}).

D. Sugimura is with the Department of Computer Science, Tsuda University, Tokyo, Japan (E-mail: sugimura@tsuda.ac.jp).

methods such as dark channel prior-based approaches [3]–[6], stereo imaging [7], and image restoration via depth estimation from the red channel [8]–[10]. In fact, methods based on their optical imaging models require accurately estimating background light [11]. Thus, it is difficult to apply them to underwater images where no background light exists.

Other statistical-based approaches have been proposed, such as Von Kries hypothesis-based histogram equalization [12], histogram equalization using mean value and mean square error [13], [14], and contrast-limited adaptive histogram equalization [15], [16]. However, these statistical-based methods cause over-emphasis or under-emphasis in underwater image correction, where only a small amount of red spectrum components can be captured.

Unlike these methods, we utilize a framework of gray information estimation for color correction (e.g., gray world [17], gray edge [18], shades of gray [19], and gray pixels [20]). In underwater images, however, it is difficult to extract reliable gray information, because gray pixels (i.e., those having the same reflectance in every color channel) in underwater images are likely to have low intensity values owing to salient attenuations in the red color component. Thus, it is difficult to discriminate between the detected gray information and image noise. Hence, the direct use of these methods is inadequate to achieve effective color correction of underwater images.

To address this problem, we capture underwater scenes by using exposure-bracketing imaging: a technique to capture multiple images with different exposure times. The long-exposure image is useful for sufficiently acquiring red spectrum information of underwater scenes. In contrast, pixel values in the green and blue channels in the long-exposure image will saturate because the green and blue components are unlikely to attenuate more than the red ones. To avoid pixel saturation of the green and blue channels, we take their pixel values from the short-exposure image. Hence, we fuse an image by selecting appropriate color channels from the captured images. This allows us to gain sufficient spectral information of scenes. Thus, our method enables us to perform efficient color correction of underwater images because gray information can be accurately extracted from the fused image.

The contributions of this study are summarized as follows. We leverage exposure-bracketing imaging to acquire sufficient spectral information of underwater scenes. Our adaptive use of multiple images taken with different exposure times allows us to accurately extract gray information from scenes. Thus, effective color correction can be achieved based on a framework of color constancy.

This paper is the extended version of our earlier study [21].

Our new contributions are as follows. First, we introduce a technique of outlier elimination, based on characteristics of underwater scenes, into the framework of gray pixel detection. Second, we introduce a linear regression approach to effectively correct color distortion using gray pixels.

II. IMAGE FUSION USING EXPOSURE-BRACKETING IMAGING

Figure 1 illustrates an overview of the proposed method. We fuse an image, including sufficient spectral information of a scene, by using multiple images taken with exposure-bracketing imaging. We perform color correction of this synthesized underwater image using gray information of scenes.

A. Image Selection

Let $\mathbf{I} = \{\mathbf{I}_1, \dots, \mathbf{I}_m, \dots, \mathbf{I}_M\}$ be a set of RGB images taken with exposure-bracketing imaging. They are taken with M different exposure times. We define each image as $\mathbf{I}_m = (\mathbf{I}_m^R, \mathbf{I}_m^G, \mathbf{I}_m^B)$. Using \mathbf{I} , we synthesize an image, \mathbf{H} , containing sufficient spectral information of underwater scenes.

Generally, it is difficult to obtain enough red spectral information from a short-exposure image because of the salient attenuations of red components. In contrast, the green and blue components will saturate in the long-exposure images. Thus, we select images that have less over- and under-exposed pixels in each color channel. For each image, $\mathbf{I}_m^l (l \in \{R, G, B\})$, we count over- and under-exposed pixels as

$$C(\mathbf{I}_m^l) = \sum_{n=1}^T \text{Bin}(\mathbf{I}_m^l(n); \sigma), \quad (1)$$

where $\mathbf{I}_m^l(n)$ is the value of the n -th pixel in \mathbf{I}_m^l ; T denotes the number of pixels of \mathbf{I}_m^l . The binary classification operator, $\text{Bin}(\cdot; \cdot)$, is defined as

$$\text{Bin}(\mathbf{I}_m^l(n); \sigma) = \begin{cases} 1 & \text{if } (\mathbf{I}_m^l(n) < \sigma) \text{ or } (\mathbf{I}_m^l(n) > U - \sigma) \\ 0 & \text{otherwise} \end{cases}, \quad (2)$$

where U is the maximum pixel value in an image. For example, if the bit depth of the image is 8, U becomes 255. Additionally, σ is a truncation parameter. The number for the image that has the least over- and under-exposed pixels for each color channel, m^l , can be estimated as

$$m^l = \arg \min_m C(\mathbf{I}_m^l). \quad (3)$$

B. Image Fusion

Exposure-bracketing imaging records multiple images with different timings. Thus, spatial misalignment between these images are observed. To compensate such misalignment, we apply a dense adaptive self-correlation descriptor (DASC) [22], which is used to estimate the visual correspondences between two images, to \mathbf{I}_{m^R} , \mathbf{I}_{m^G} , and \mathbf{I}_{m^B} . Typically, the compensation accuracy of spatial misalignment between two images decreases when the shooting times are largely different from one another. To mitigate deterioration of performance of visual correspondences, we set the reference image as the one taken at the median timing m^{md} among \mathbf{I}_{m^R} , \mathbf{I}_{m^G} , and \mathbf{I}_{m^B} . Therefore, the aligned image $\hat{\mathbf{I}}_{m^l}$ can be obtained as

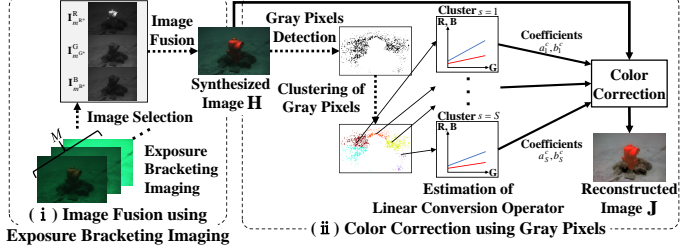


Fig. 1. Overview of the proposed method: (i) image fusion using exposure-bracketing imaging; (ii) color correction using gray pixels.

$$\hat{\mathbf{I}}_{m^l} = \mathcal{D}(\mathbf{I}_{m^l}, \mathbf{I}_{m^{\text{md}}}) \text{ for } m^l \neq m^{\text{md}}, \quad (4)$$

where $\mathcal{D}(A, B)$ represents an image registration operator that aligns image A with B ; it is computed by DASC. Using the aligned images, we synthesize $\mathbf{H} = (\mathbf{H}^R, \mathbf{H}^G, \mathbf{H}^B)$ as

$$\mathbf{H}^l = \begin{cases} \hat{\mathbf{I}}_{m^l} & \text{if } m^l \neq m^{\text{md}} \\ \mathbf{I}_{m^{\text{md}}} & \text{otherwise.} \end{cases} \quad (5)$$

III. COLOR CORRECTION USING GRAY PIXELS

A. Gray Pixel Detection with Outlier Elimination

We first detect gray pixels, $\mathbf{X} = \{\mathbf{x}_i\}_{i=1,\dots,N}$, by using the method referenced in [20]. In our method, to improve the accuracy of gray pixel detection in underwater images, we introduce a scheme for elimination of outlier gray pixels based on characteristics of light attenuation in underwater scenes.

In underwater scenes, the amount of color distortion changes gradually depending on light propagation distance. Thus, we suppose that the gray pixels are likely to distribute continuously in the RGB color space. We consider outliers to be gray pixels that are isolated in the RGB color space.

We perform outlier elimination based on the proximities of gray pixels in the RGB color space. Specifically, we utilize the following iterative procedure.

Let $\mathbf{Z}^{(k)} = \{\mathbf{z}_i^{(k)}\}_{i=1,\dots,N_k}$ be a set of gray pixels that are classified as the correct ones at the k -th iteration. Additionally, we define a subset of \mathbf{X} that is not evaluated at the k -th iteration as $\mathbf{Y}^{(k)} = \{\mathbf{y}_i^{(k)}\}_{i=1,\dots,N-N_k}$ (i.e., $\mathbf{Y}^{(k)} = \mathbf{X} \setminus \mathbf{Z}^{(k)}$). We iteratively update $\mathbf{Z}^{(k)}$ until $\mathbf{Y}^{(k)} = \emptyset$. Below, we describe details of this iterative procedure.

1) Initial Step: We assume that many components in \mathbf{X} can be detected correctly because the fused image, \mathbf{H} , includes sufficient spectral scene information. Based on this assumption, we consider that the gray pixels that are close to the centroid of \mathbf{X} in the RGB color space would be the correct ones. Based on this assumption, we obtain $\mathbf{Z}^{(0)}$ as

$$\mathbf{Z}^{(0)} = \{\mathbf{x}_i \mid \|\mathbf{x}_i - \mathbf{o}\|_2 < th\}, \quad (6)$$

where \mathbf{o} is the centroid of \mathbf{X} in the RGB color space; th is a threshold; and $\|\cdot\|_2$ denotes ℓ_2 norm. We then obtain $\mathbf{Y}^{(0)}$ as $\mathbf{Y}^{(0)} = \mathbf{X} \setminus \mathbf{Z}^{(0)}$.

2) Iteration: Based on the assumption of which correct gray pixels would be continuously distributed in the RGB color space, we evaluate $\mathbf{Y}^{(k-1)}$ by measuring the proximities between $\mathbf{Y}^{(k-1)}$ and $\mathbf{Z}^{(k-1)}$. Specifically, $\mathbf{Z}^{(k)}$ is updated as

$$\mathbf{Z}^{(k)} = \mathbf{Z}^{(k-1)} + \{\mathbf{y}_i^{(k-1)} \mid \|\mathbf{y}_i^{(k-1)} - \mathbf{z}_j^{(k-1)}\|_2 < th\}. \quad (7)$$

Like the initial procedure, $\mathbf{Y}^{(k)}$ is updated as $\mathbf{Y}^{(k)} = \mathbf{X} \setminus \mathbf{Z}^{(k)}$.

After this iterative processing, we obtain a set of gray pixels, \mathbf{Z} , that are used for color correction.

B. Color Correction of Fused Image

Using \mathbf{Z} , we perform color correction of \mathbf{H} . In a canonical illumination environment, gray pixel has the same intensity value for all the color channels (i.e., RGB). In addition, there are linear relationships between each color channel with respect to changes in the pixel intensity. We use the characteristics of gray pixels as a prior for color correction of underwater images.

1) *Scene Clustering*: As described earlier, color distortions of underwater images vary spatially. Thus, the linear relationships of gray pixels between color channels will also be different depending on regions in the image. To adaptively correct color distortions of underwater images, we first perform k -means clustering of \mathbf{Z} to divide \mathbf{H} into S regions, $\mathbf{H}_1, \dots, \mathbf{H}_S$, as was done in the previous color-correction method [20]. We utilize a spatial proximity (i.e., Euclidean distance in the image) and a color similarity (i.e., Euclidean distance in the RGB color space) between components of \mathbf{Z} as criteria for clustering processing. We define a subset of gray pixels that belong to the s -th cluster as $\mathbf{Z}_s = \{\mathbf{z}_{s,1}, \dots, \mathbf{z}_{s,N_s}\}$.

2) *Estimation of Linear Conversion Operator*: We consider that gray pixels belonging to the same cluster will have a similar amount of color distortions. Hence, we estimate the linear relationships of gray pixels for each cluster. We estimate a linear conversion operator for color correction, such that red and blue intensity values align with the same as that of green channel. Based on the linear relationships between each color channel, we model the relation between green and the other channels as

$$\mathbf{z}_{s,t}^c = a_s^c \mathbf{z}_{s,t}^G + b_s^c \quad c \in \{\text{R, B}\}, \quad t = 1, \dots, N_s, \quad (8)$$

where a_s^c and b_s^c are coefficients of linear conversion for the s -th cluster. We apply a linear principal component regression to \mathbf{Z}_s to estimate a_s^c and b_s^c .

3) *Color Correction*: With the estimated coefficients of linear conversion, a_s^c and b_s^c , we perform color correction of \mathbf{H} . We then obtain color-corrected underwater image, $\mathbf{J} = (\mathbf{J}^{\text{R}}, \mathbf{J}^{\text{G}}, \mathbf{J}^{\text{B}})$. In this processing, we assume that the linear conversions that are close to the position of target pixel, \mathbf{p} , will effectively contribute to the color correction for the pixel value, $\mathbf{H}(\mathbf{p})$. Thus, we define the weight, $w_s(\mathbf{p})$, as

$$w_s(\mathbf{p}) = \exp\left(-\frac{1}{2\alpha^2} \frac{\|\mathbf{p} - \mathbf{p}_s\|_2^2}{\sqrt{W^2 + H^2}}\right), \quad (9)$$

where α is a parameter that controls weighting sensitivity. Additionally, \mathbf{p}_s denotes a position of gray pixel in the s -th cluster that is the closest to \mathbf{p} . The image resolutions with respect to horizontal and vertical directions are represented as W and H , respectively.

With the weight, $w_s(\mathbf{p})$, we correct color distortion of $\mathbf{H}(\mathbf{p})$ based on mixture of the weighted linear conversions. We compute the color-corrected image for each channel as

$$\mathbf{J}^c(\mathbf{p}) = \frac{1}{\mu} \sum_{s=1}^S w_s(\mathbf{p}) \frac{\mathbf{H}_s^c(\mathbf{p}) - b_s^c}{a_s^c}, \quad (10)$$

where $\mu = \sum_s w_s$ is a normalization coefficient.

IV. EXPERIMENTAL RESULTS

We tested the proposed method using six raw underwater images taken at various water depths (from -12 to -30 meters). Since spectral sensitivities of digital cameras are typically designed so as to have high sensitivities in the green wavelength band, raw images seem to be greenish. However, we can consider that the amount of attenuation of red spectrum components is different between these images because they were captured at various water depths. We named them "S1," ..., "S6," respectively. We captured images by using a Sony Cyber-shot RX100M5 with the AutoExposure-Bracketing mode, which automatically sets the exposure times of captured images. The number of images taken with this exposure-bracketing imaging to nine ($M = 9$).

Parameters used in the proposed method were set such that S varied from 1 to 5, th varied from 0.07 to 1, $\sigma = 3.9$, and $\alpha = 0.2$. Because σ is a parameter to determine over- and under-exposed pixels in an image, we consider that it depends on a camera specification. However, it is difficult to determine an optimal σ from publicly available camera specification information. Hence, we determined σ empirically by analyzing color histograms of over- and under-exposed underwater images in the preliminary experiments. For α , we set the same value as that reported in the previous method [20]. We observed that varying α made little difference in the resulting color-corrected images. On the other hand, we observed that the setting of S and th influenced the resulting color-corrected images. Hence, we analyzed the color correction performance by varying S and th (Sec. IV-B).

Our experiments were run on a Windows PC with an Intel Core i7-6700 3.4GHz, and we used Matlab R2017a. The processing time for our computation without optimizing implementations was approximately 350 seconds. In our computation, image fusion using DASC method [22] is the most time-consuming part, it costs approximately 160 seconds.

A. Comparisons with State-of-the-art Methods

We compared the proposed method with state-of-the-art methods. In this comparison, we used five other methods for underwater image enhancement [5], [23], [12], [24], and [13]. We also compared our method with our prior algorithm, proposed in [21]. In addition, because our method is based on gray information estimation, we evaluated the performance of other gray information-based methods [17], [20]. We used a fused image \mathbf{H} as input for our method and for [21]. For the other comparison methods, we used $\mathbf{I}_{m^{\text{md}}}$ as input.

To quantitatively compare the color correction performance of our method with that of the other methods, we placed two color checker boards in scenes S1 through S4. In these scenes, one checker board was located near to the camera, whereas the other was positioned far from the camera. We denote them "Near" and "Far," respectively. In this quantitative evaluation, we adopted CIEDE 2000 [25], which is a metric that measures color differences between two images.

Table I shows the quantitative comparison results of CIEDE 2000 values. Figure 2 shows qualitative comparisons of the

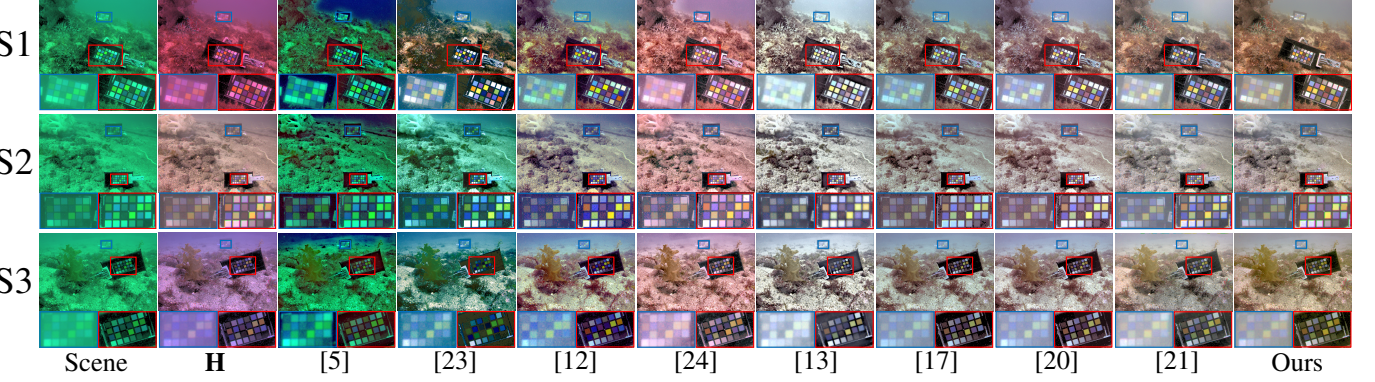


Fig. 2. Visual comparisons in color correction of underwater images. Note that the scene images were obtained interpolating taken raw images.

reconstructed underwater images for three scenes. As shown in Table I and Fig. 2, we observed that our method outperformed the other comparison methods in many scenes. Consequently, we can state that the proposed method has better performance compared to that of the other methods.

B. Discussion: Influences with Varying S and th

We analyzed the influences of varying S and th in color correction of underwater images. We used S1 and S2 for this evaluation. We varied them such that $0.26 \leq th \leq 0.39$ and $1 \leq S \leq 9$.

Figure 3 shows changes in the CIEDE 2000 values with varying S and th . We see that our results with varying S and th compared favorably with that of the other comparison methods shown in TABLE I. However, we also observed that the color correction performance varied.

As described in Sec. III-B, we divide an input image into S regions to adaptively correct spatially-varying color distortions. This indicates that the choice of S affects the color correction performance. We think that another clustering procedure that automatically estimates the number of clusters (e.g., [26], [27]) would be useful to suppress variations in the color correction performance.

The parameter th controls how much the detected gray pixels are used for the color correction of underwater images (Sec.III-A). If we set a higher value for th , many outliers will be accepted. In contrast, few gray pixels are employed for color corrections if we set a lower value for th . In other words, accurate gray pixels are wrongly classified as outliers. Because of the above reason, we think that the choice of th influenced the performance of color correction. To address this problem, we will use spatial variance of detected gray pixels as criteria to achieve accurate outlier elimination as in [28].

C. Analysis of Contrast Enhancement Performance

As mentioned earlier, the objective of this study is to perform color correction of underwater images. However, the goal of underwater image enhancement is to correct color distortions, but also recovering contrast of images. Hence, we evaluated the performance of contrast enhancement by using the histogram entropy measure. We measured it for the reconstructed image entirely.

Table II shows the quantitative comparison results of the histogram entropy measure. We observed that our results were

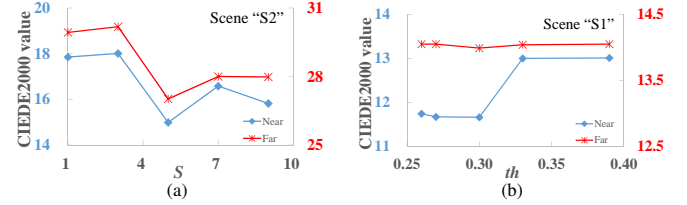


Fig. 3. Changes in the CIEDE 2000 values with varying (a) S and (b) th . We measured them in **Near** (blue line) and **Far** (red line) regions, respectively.

TABLE I
COMPARISONS IN CIEDE2000 VALUES. NOTE THAT THESE VALUES ARE MEASURED USING THE PIXEL VALUES OF REGIONS OF THE COLOR CHECKER BOARDS. BEST SCORES ARE REPRESENTED IN **BOLD**.

	[5]	[23]	[12]	[24]	[13]	[17]	[20]	[21]	Ours
S1(Near)	52.13	20.63	17.41	22.82	23.84	14.59	16.31	12.63	11.66
S1(Far)	55.69	15.32	18.98	24.08	30.00	17.81	17.48	14.44	13.99
S2(Near)	52.34	28.23	20.80	22.72	23.13	18.34	19.19	15.10	14.99
S2(Far)	41.52	50.51	33.53	28.00	29.56	27.40	27.05	27.48	27.02
S3(Near)	35.52	43.03	26.04	16.37	19.66	16.75	16.40	16.15	15.46
S3(Far)	57.11	31.86	29.37	21.66	24.94	24.07	23.84	18.65	19.02
S4(Near)	52.95	25.50	19.50	20.17	23.01	14.35	15.80	13.84	12.83
S4(Far)	55.90	31.58	19.84	20.27	23.65	19.29	19.77	16.41	14.31

TABLE II
COMPARISONS IN HISTOGRAM ENTROPY MEASURES. BEST SCORES ARE REPRESENTED IN **BOLD**.

	[5]	[23]	[12]	[24]	[13]	[17]	[20]	[21]	Ours
S1	6.864	7.136	7.072	7.584	7.724	6.573	7.340	7.175	7.016
S2	6.979	7.725	7.070	7.536	7.685	6.421	7.393	6.976	6.937
S3	7.343	7.566	7.386	7.634	7.711	6.984	7.459	7.196	7.181
S4	6.987	7.358	7.526	7.623	7.705	7.083	7.457	7.510	7.428
S5	7.357	6.601	7.527	7.690	7.672	7.294	7.607	7.391	7.357
S6	7.368	7.750	6.950	7.711	7.740	7.431	7.223	7.343	7.538

inferior than those obtained using the methods [13], [23], [24]. This is primarily because these methods performed haze removal as well as color correction. In contrast, our method only performed color correction of underwater images; no contrast enhancement processing was performed. In the future research, we will explore techniques of contrast enhancement.

V. CONCLUSION

We proposed a method for color correction of underwater images. We exploited exposure-bracketing imaging to fuse an image that includes sufficient spectral information of underwater scenes. We performed color correction based on a linear regression of the extracted gray pixels. Experimental results showed the superiority of our color correction method over the comparison methods. We also discussed the limitations to our current method. In the future research, we will address the remaining problems as well as exploring contrast enhancement techniques.

REFERENCES

- [1] S. Q. Duntley, "Light in the sea," *OSA JOSA*, vol. 53, no. 2, pp. 214–233, 1963.
- [2] H. Koschmieder, "Theorie der horizontalen sichtweite," *Beitrage zur Physik der freien Atmosphare*, pp. 33–53, 1924.
- [3] K. He, J. Sun, and X. Tang, "Single image haze removal using dark channel prior," *IEEE TPAMI*, pp. 2341 – 2353, 2010.
- [4] P. Drews, E. do Nascimento, F. Moraes, S. Botelho, and M. Campos, "Transmission estimation in underwater single images," in *Proc. of IEEE ICCV*, 2013, pp. 825–830.
- [5] H. Wen, Y. Tian, T. Huang, and W. Gao, "Single underwater image enhancement with a new optical model," in *Proc. of IEEE ISCAS*, 2013, pp. 753–756.
- [6] J. Y. Chiang and Y. C. Chen, "Underwater image enhancement by wavelength compensation and dehazing," *IEEE TIP*, vol. 21, no. 4, pp. 1756 – 1769, 2012.
- [7] S. Zhang, J. Zhang, S. Fang, and Y. Cao, "Underwater stereo image enhancement using a new physical model," in *Proc. of IEEE ICIP*, 2014, pp. 5422–5426.
- [8] N. C. Bianco, A. Mohan, M. R. Eustice, and A. Arbor, "Initial results in underwater single image dehazing," in *Proc. of IEEE OCEANS*, 2010, pp. 1–8.
- [9] Y. T. Peng and P. C. Cosman, "Underwater image restoration based on image blurriness and light absorption," *IEEE TIP*, vol. 26, no. 4, pp. 1579–1592, 2017.
- [10] C. Y. Li, J. C. Guo, R. M. Cong, Y. W. Pang, and B. Wang, "Underwater image enhancement by dehazing with minimum information loss and histogram distribution prior," *IEEE TIP*, vol. 25, no. 12, pp. 5664–5677, 2016.
- [11] Y. Wang, H. Liu, and L. P. Chau, "Single underwater image restoration using adaptive attenuation-curve prior," *IEEE TCSVT*, vol. 65, no. 3, pp. 992–1002, 2017.
- [12] K. Iqbal, M. James, R. A. Salam, and A. Z. H. Talib, "Enhancing the low quality images using unsupervised colour correction method," in *Proc. of IEEE SMC*, 2010, pp. 1703–1709.
- [13] X. Fu, P. Zhuang, Y. Huang, Y. Liao, and X. P. Zhang, "A retinex-based enhancing approach for single underwater image," in *Proc. of IEEE ICIP*, 2014, pp. 4572–4576.
- [14] J. Yang, X. Wang, H. Yue, X. Fuz, and C. Houy, "Underwater image enhancement based on structure-texture decomposition," in *Proc. of IEEE ICIP*, 2017, pp. 1207–1211.
- [15] M. S. Hitam, W. N. Jawahir, H. W. Yuss, E. A. Awalludin, and Z. Bachok, "Mixture contrast limited adaptive histogram equalization for underwater image enhancement," in *Proc. of IEEE ICCAT*, 2013, pp. 1–5.
- [16] W. N. J. H. W. Yussof, M. S. Histam, E. A. Awalludin, and Z. Bachok, "Performing contrast limited adaptive histogram equalization technique on combined color models for underwater image enhancement," *IJIDM*, vol. 1, no. 1, pp. 1–6, 2013.
- [17] G. Buchsbaum, "A spatial processor model for object colour perception," *Journal of The Franklin Institute*, vol. 310, pp. 1–26, 1980.
- [18] J. V. D. Weijer and T. Gevers, "Color constancy based on the grey-edge hypothesis," in *Proc. of IEEE ICIP*, 2005, pp. II–722.
- [19] G. D. Finlayson and E. Trezzi, "Shades of gray and colour constancy," in *Proc. of IS&T/SID Color Imaging Conference*, 2004, pp. 37–41.
- [20] K. F. Yang, S. B. Gao, and Y. J. Li, "Efficient illuminant estimation for color constancy using gray pixels," in *Proc. of IEEE CVPR*, 2015, pp. 2254–2263.
- [21] K. Nomura, D. Sugimura, and T. Hamamoto, "Color correction of underwater images based on multi-illuminant estimation with exposure bracketing imaging," in *Proc. of IEEE ICIP*, 2017, pp. 705–709.
- [22] S. Kim, D. Min, B. Ham, M. N. Do, and K. Sohn, "Dasc: Robust dense descriptor for multi-modal and multi-spectral correspondence estimation," *IEEE TPAMI*, vol. 39, no. 9, pp. 1712–1729, 2017.
- [23] D. Berman, T. Treibitz, and S. Avidan, "Diving into haze-lines: color restoration of underwater images," in *Proc. of BMVC*, 2017.
- [24] C. Ancuti, C. O. Ancuti, T. Haber, and P. Bekaert, "Enhancing underwater images and videos by fusion," in *Proc. of IEEE CVPR*, 2012, pp. 81–88.
- [25] M. R. Luo, G. Cui, and B. Rigg, "The development of the cie 2000 colour-difference formula: Ciede2000," *WILEY CRA*, vol. 26, no. 5, pp. 340–350, 2001.
- [26] D. Pelleg and A. Moore, "X-means: extending k-means with efficient estimation of the number of clusters," in *Proc. of ICML*, 2000, pp. 727–734.
- [27] B. J. Frey and D. Dueck, "Clustering by passing messages between data points," *Science*, vol. 315, no. 5814, pp. 972–976, 2007.
- [28] R. B. Rusu, N. Blodow, Z. Marton, A. Soos, and M. Beetz, "Towards 3d object maps for autonomous household robots," in *Proc. of IEEE/RSJ IROS*, 2007, pp. 3191–3198.